IEEE Access
Multidisciplinary | Rapid Review | Open Access Journal

Date of publication xxxx 00, 0000, date of current version Jun 15, 2023.

Digital Object Identifier 10.1109/ACCESS.2023.0322000

Fast and simple statistical shape analysis of pregnant women using radial deformation of a cylindrical template

LIKHIT K. NAYAK[1], (Member, IEEE), MAHLET Y. GEBREMARIAM[2], Elianna Paljug[3], and Rudolph L. Gleason, Jr.[1, 4],

[1]The George W. Woodruff School of Mechanical Engineering, Georgia Institute of Technology, Atlanta, GA, 30332 USA (e-mail: lnayak3@gatech.edu)
[2] Department of Obstetrics & Gynecology, Addis Ababa University, Addis Ababa, Ethiopia (e-mail: gyobmahi@gmail.com)
[3]Hubert Department of Global Health, Rollins School of Public Health, Emory University, Atlanta, 30322 GA (email: elianna.paljug@emory.edu)
[4]The Wallace H. Coulter Department of Biomedical Engineering, Georgia Institute of Technology, Atlanta, GA, 30332 USA (email: rudy.gleason@me.gatech.edu)

Corresponding author: Rudolph L. Gleason, Jr. (e-mail: rudy.gleason@me.gatech.edu).

This work was supported by National Institutes of Health (NIH) grant 5R01HD100635-03.

ABSTRACT Non-rigid deformation of a template to fit 3D scans of human subjects is widely used to develop statistical models of 3D human shapes and poses. Complex optimization problems must be solved to use these models to parameterize scans of pregnant women, thus limiting their use in antenatal point-of-care tools in low-resource settings. Moreover, these models were developed using datasets that did not contain any 3D scans of pregnant women. In this study, we developed a statistical shape model of the torso of pregnant women at greater than 36 weeks of gestation using fast and simple vertex-based deformation of a cylindrical template constrained along the radial direction. The 3D scans were pre-processed to remove noisy outlier points and segment the torso based on anatomical landmarks. A cylindrical template mesh T was then fitted onto the segmented scan of the torso by moving each vertex of T in the direction of the radial vector. This process is computationally inexpensive taking only 14.80 seconds to deform a template with 9090 vertices. Principal component analysis (PCA) was performed on the deformed vertex co-ordinates to find the directions of maximum variance. The first 10 principal vectors of our model explained 79.03% of the total variance and reconstructed unseen scans with a mean error of 2.43 cm. We also used the PCA weights of the first 10 principal vectors to accurately predict anthropometric measurements of the pregnant women.

INDEX TERMS Anthropometry, CPD, non-rigid deformation, pregnancy, point-of-care, radial deformation, SSA, template fitting.

I. INTRODUCTION

THE ease of use, accuracy, and precision of 3D scanning technologies [1], [2] have made them increasingly popular as a tool for obtaining reliable anthropometric measurements. Conventional anthropometry suffers from several drawbacks, such as large measurement errors, poor reliability [3], operator-to-operator variability [2], and the long time required to collect multiple measurements. Digital anthropometric tools address these drawbacks and have been shown to be faster while having higher reliability and precision [1], [2], [4]. These tools are used to collect traditional anthropometric measurements such as height or body circumference. However, the definitions of these measurements are often unclear because of proprietary software and are unique to each manufacturer [5], making it difficult to leverage the potential of 3D data to develop universal prognostic models that can be used as clinical interventions.

Low-cost, handheld 3D scanners have been validated for recording various anthropometric measurements, such as height, body circumference and body volume [6]–[8]. In biological anthropology, landmarks and semilandmarks are used to analyze shape variations of specific anatomical regions using 3D geometric morphometrics [9]. These landmarks are either detected manually [7], [9] or estimated automatically from the scan [6]–[8], [10]. Manual detection of landmarks is time-consuming and the presence of noise and holes in raw scans make automated landmark detection challenging. Previous studies have used non-rigid vertex-based deformations of predefined templates to obtain clean scans [11]–[15]. An additional benefit of template deformation is the standardization of mesh topology across all participants making it easy to develop a statistical shape model. This model could

also enable accurate and automatic detection of homologous anatomical landmarks and semilandmarks for 3D geometric morphometrics. The predefined templates can be custom-generated [11], [12] or derived from existing models such as SCAPE [16] or SMPL [17], and undergo shape deformation and pose deformation to fit the observed scan [18]. However, solving these deformation parameters is computationally expensive and can take hours on point-of-care tools that include smartphones and tablets.

Maternal anthropometric measurements constitute an important component of the WHO (World Health Organization) guidelines for antenatal care, especially as a metric for characterizing under-nutrition [19]. These measurements have also been effective in predicting risk of cephalopelvic disproportion (CPD) [6], [20], [21]. CPD is a mismatch in the size of the maternal pelvis and fetal head that often leads to obstructed labor and requires delivery by Cesarean section (C/S) [20]. Emergency C/S facilities are rarely available to women living in low-resource settings and a lack of timely access to these facilities leads to a higher incidence of maternal and perinatal mortality due to CPD-related obstructed labor [6], [20]. Maternal anthropometric measurements have been strongly linked with pregnancy outcomes [6], [20]–[23], and analyzing 3D shape variations in pregnant women could help determine the risk of CPD in the early stages of gestation. This would enable high-risk women to be referred early to healthcare facilities where emergency C/S is available. Existing parametric models of human shape [16], [17] are learned on large publicly available data-sets of 3D scans [12], [24], [25], which do not include any data from the pregnant population. This makes it challenging to use these models to characterize shape variations in pregnant women. Even though there are pregnancy-related shape models that use MRI or ultrasound data to characterize specific structures, such as the uterus or the pelvic floor [26], [27], there is a strong need for a statistical model that characterizes the morphological shape of pregnant women using 3D scans.

The objective of this study was to address these gaps and we make two novel contributions to that end. First, we introduce a simple, constrained optimization to parameterize 3D scans, which is computationally inexpensive and can be performed on standard tablets and smartphones, enabling its use as a point-of-care tool for routine antenatal care. Second, we developed a statistical model to represent the shape variations of the torso of pregnant women, at or near term. Our model used the radial deformation of a cylindrical template mesh to fit the observed 3D scan (Fig. 1). Each vertex of the template was constrained to move in the radial direction, making it easy to solve the optimization problem. The methods and model presented in this study can be used to characterize, in real-time, the morphological shape variations in the pregnant population which can then be correlated with the risk of adverse maternal outcomes like CPD.

II. METHODS

A. COLLECTION OF 3D SCANS FROM PARTICIPANTS

Data collection was approved by the Institutional Review Board (IRB) at Addis Ababa University, College of Health Sciences (Protocol number: 054/15/gyn) and the Georgia Institute of Technology IRB (Protocol number: H19320). In this study, we used 225 3D scans of primigravida women, aged between 18 and 40 years, with singleton pregnancies collected after 36 weeks of gestation. Following previously described methods, 3D meshes were collected by trained nurses using a Structure 3D Sensor (Occipital, Inc.) across two health facilities (Woreda 11 Health Center and Gandhi Memorial Hospital) in Addis Ababa, Ethiopia [6]. The participants were asked to remove any loose clothing items and stand with their arms lifted to at least 45◦, and their feet were placed approximately 50 cm apart (Fig. 2). Participants with hair extending beyond the shoulder were asked to tie it up to prevent occlusion of the back or shoulders (Fig. 3). The time taken by a trained nurse to collect a 3D scan using this method was between 3 to 5 minutes. Along with the 3D scans, eight anthropometric measurements were collected for each participant: height, weight, shoulder width, shoulder height, waist circumference, waist height, hip circumference, and trochanteric height using previously described methods [6]. To assess inter-user variability, 12 additional participants were recruited with the same demographics as described above. For each participant, 3D scans and anthropometric measurements were obtained by three different trained nurses. The 3D mesh processing, template fitting, and subsequent statistical analysis were all performed on a MacBook Pro (Apple, Inc.) with an Apple M1 chip and 16 GB RAM.

B. MESH PRE-PROCESSING

Raw scans were processed to remove outlier objects along with the floor plane. The approximate positions of the left and right armpits, left and right shoulders, and groin were marked manually on each scan. These landmarks were used to segment the scan into five regions (Fig. 4). All regions except the torso were removed. Each scan was then rotated to a frontal position and normalized to fit a unit sphere centered at origin as follows:

$$v_i = \frac{v_i - \mu_S}{max||v_i - \mu_S||_2}, \tag{1}$$

where v_i is the i^{th} vertex of segmented scan S, μ_S is the centroid of S, and $||.||_2$ represents the $L2$ norm.

C. RADIAL DEFORMATION OF CYLINDRICAL TEMPLATE

Cylindrical template mesh T was deformed to fit the segmented scanned mesh S, as shown in Fig. 1. Template T, with a unit radius and height of two units, was centered at the origin and oriented in the y-direction. The number of vertices N_T of T was controlled by two factors: (i) the differential angle $\Delta\theta_r$ (in degrees) subtended at the centerline of the cylinder by neighboring vertices on the same xz plane, as shown in Fig. 5a, and (ii) the cross-sectional distance Δy between individual xz planes along the y-axis, as shown in Fig. 5b. Template T

was compressed uniformly along the y-axis to align with the height of S. This is followed by deformation of each vertex $x_i, i = 1, 2, ...N_T$ of T given by

$$x_i = x_i + t_i r_i, \tag{2}$$

where r_i is the direction of the radial vector from x_i towards the centerline of the cylinder along the xz plane and t_i is the radial deformation, that is, the shortest distance between x_i and the front-facing surfaces of S along r_i. Radial deformation was calculated using the Moller-Trumbore algorithm [28], which efficiently checks for ray-face intersections in three-dimensions. If the scan had holes along the surface (Fig. 6), some of the radial rays would pass through S without intersecting any face. The radial deformations of these vertices were calculated by iteratively averaging the radial deformations of the neighboring vertices.

Radial deformation of the cylindrical mesh was implemented for six different values of N_T. The average time taken for each deformation and the average error between the deformed template $T^{'}$ and original scan S were calculated for each N_T. The reconstruction error E_R is given by

$$E_R = \frac{\sum_{i=1}^{N_T} ||x_i - v_i^S||_2 - \sum_{i=1}^{N_S} ||x_i^T - v_i||_2}{N_T + N_S}, \tag{3}$$

where N_S is the total number of vertices in S, y_i^S is the closest point in S to x_i and x_i^T is the closest point in deformed template $T^{'}$ to y_i.

D. STATISTICAL MODELLING OF SHAPE VARIATIONS

To develop the statistical model, the data-set was randomly divided into training (n=180) and testing set (n=45). This was done to demonstrate the ability of our model to generalize to unseen scans, i.e., the scans in the testing set. The x, y, and z co-ordinates of the deformed template vertices in the training set were concatenated into 180 vectors, each of length $3N_T$. N_T was chosen to be 9090. Principal component analysis (PCA) was then performed on these vectors to determine the directions of maximum variance. To test the model, the reconstruction error was calculated for the scans in the testing set using the first 10, 25, 50, and 100 principal vectors, according to (3). In addition, we also developed and tested the statistical shape model using the metrics of compactness, generalization, and specificity for the first 10, 25, 50, and 100 principal vectors [29]. The compactness of the model, which was developed using all the 225 scans, was defined as the ratio of the total variance explained by the principal vectors. The generalization error was calculated using leave-one-out cross-validation for all the 225 scans [30] and the specificity was calculated as the average minimum distance of uniformly distributed, randomly generated scans (n=100) from the training set (n=225) [29].

We also trained a linear regression model to find a function $f(p_i) \rightarrow a_i$ that maps a set of PCA weights p_i to a set of anthropometric measurements a_i. The weights for the first 10 principal vectors of the training set were taken as the independent variable for $f(p_i)$ and the dependent variable was the set of eight anthropometric measurements collected for each participant. The cube root of the weight was used for the regression model to make it comparable to the other measurements because the weight is roughly proportional to volume [11]. The inter-user variability of the trained regression model was compared with that of anthropometric measurements obtained by trained nurses using a tape measure. The variability of the measurements was defined as the standard deviation between repeated measurements of the same participant (n=12). To obtain the predicted anthropometric measurements, a cylindrical template (N_T=9090) was deformed to fit the three different 3D scans of each participant. The weights of the first 10 principal vectors of the deformed vertices were then used to predict the anthropometric measurements. All comparisons of significance were performed using two-tailed T-tests.

III. RESULTS

The time taken for our template deformation increased almost linearly with an increase in N_T (Table I). The average deformation error also showed a generally decreasing trend with increasing N_T and started to plateau beyond N_T=36000. Decreasing the cross-sectional distance Δy beyond 0.01 units, while keeping N_T nearly constant leads to an increase in the deformation error (Table I). This could be attributed to the intrinsic resolution of S which is a function of the scanning device. The first 10 principal vectors of the trained PCA shape model explained 79.1% of the total variance. This increased to 90.4%, 95.3%, 98.3% for the first 25, 50 and 100 principal vectors, respectively. The major principal directions of the developed model are shown in Fig. 7. The first principal vector affects the curvature of the spine and bust size. The second principal vector affected the torso circumference and the length of the torso and the third principal vector influenced the hip size as well as the torso length. These vectors were then used to successfully reconstruct the unseen scans, i.e., the scans in the testing set ($n = 45$). As expected, the mean reconstruction error decreased when the number of principal vectors k increased (Table II). The largest decrease was observed when k was increased from 10 to 25. The reconstruction is visualized using Hausdorff distance (Fig. 8) and by overlaying the reconstructed scans on the original ones (Fig. 9). The compactness, generalization and specificity of the model is shown in Table III. As the number of principal vectors increase, the model becomes more compact and generalizes better but the specificity error increases (Table III).

The average error (%) between the actual and predicted anthropometric measurements is shown in Table IV. The average error for all predicted measurements, except for the weight, was below 5%. No improvement was observed in the average error % after increasing the number of vertices, N_T, of the cylindrical template. The predicted measurements of shoulder width, waist height and trochanteric height showed a significant reduction ($p < 0.005$) in inter-user variability when compared to the actual measurements taken using the tape measure (Fig. 10). No significant differences were ob-

served in the inter-user variability of the other anthropometric measurements.

IV. DISCUSSION

Existing 3D shape models of the human body use both shape and posture parameters to characterize the variations observed in the human population [12], [16], [17]. Owing to the complexity of the human pose and shape, these models require solving expensive optimization problems to obtain the deformation parameters. In addition, these models have been trained on datasets [12], [24], [25] that do not include any 3D scans of pregnant women. In this paper, we present the first statistical shape model to characterize morphological variations in a pregnant population.

Our shape model focuses only on the torso regions of the participants. Pose-related parameters have little prognostic value for assessing the risk of adverse events in the pregnant population. In the standing posture, these parameters are primarily affected by the differences in the positioning of the arms and legs (Fig. 2). To eliminate the effect of these parameters on our model, we segmented the arms and legs. We also removed the head and neck region to prevent facial or hairstyle variations (Fig. 3) from affecting the model. The segmented torso region might still be affected by pose-related variations arising from presence of quasi-similar postures [30]. The choice of cylindrical template was inspired by previous studies [31], [32], which used either cylinders or truncated cones as part of the template to model the human shape. The constrained radial deformations used for developing the model assume that the transverse plane of the scan is perpendicular to the y-axis. This is a reasonable assumption considering the average tilt of the floor plane with respect to the y-axis was 0.61 degrees for the 225 scans and the maximum tilt angle was 1.67 degrees. The regularization term used in previous vertex-based deformation models [11], [12], [18] is also omitted because our proposed deformation is not isometric. This further simplifies the optimization process. The results also demonstrate smooth surfaces without requiring any additional constraints, as shown in Fig. 1, Fig. 5 and Fig. 6. Our proposed deformation is quick, taking only 14.80 seconds to deform 9090 vertices, and can potentially be used in point-of-care applications.

The statistical shape model successfully characterizes the variations observed in 3D scans of the torso of pregnant women. The model accurately reconstructs most regions of the torso, except the region between the belly and the hip and areas with higher curvature such as the sides of the breast (Fig. 8).

In future studies, we plan to use the radial deformation and the statistical shape model for assessing the risk of CPD. The radial deformation allows us to encode any mesh as a vector of length N_T, consisting of the radial distances of the mesh from a fixed cylinder. This encoding can potentially be used as a feature vector for predicting the risk of CPD. The PCA vectors obtained from the statistical shape model represent the morphological shape of a pregnant woman and previous studies have successfully used morphological features to predict CPD [6], [20]–[23]. We could use these vectors, individually or in combination with the radial encoding, as inputs to a model that would determine the probability that a pregnant woman develops CPD during labor.

The PCA vectors of our deformation model served as features for predicting anthropometric measurements using linear regression. The predicted values for all measurements, except the weight, closely matched with the actual measurements. For two different values of N_T, the height prediction had the minimum error and the hip circumference prediction had the maximum error. The prediction error was not affected by the number of vertices, N_T, of cylindrical template T. The poor prediction of weight the can be attributed to the fact that we used only the torso region to develop our model. The predicted anthropometric measurements also showed lower inter-user variability compared to traditional anthropometric measurements obtained using a tape measure. The predicted measurements of shoulder width, waist height, and trochanteric height showed significantly reduced inter-user variability (Fig. 10). Our proposed model can be used as a more reproducible alternative to traditional tape measurements for collecting maternal anthropometric data.

The model proposed in this study has several limitations. First, it was developed using a small data-set of only 225 scans. A larger dataset would allow the model to capture a wider range of variations and improve the prediction of anthropometric measurements. Furthermore, the use of PCA on a small set of training scans prevents the model from fully spanning the high-dimensional space of non-rigid transformations [33]. This can be addressed in future work by incorporating alternative strategies like wavelet-based decomposition coupled with PCA [33]. Second, the model characterizes the shape variations of only the torso region using a cross-sectional encoding. Performing PCA directly on the cross-sectional encoding prevents the statistical shape model from being isometric-invariant. The model cannot be extended robustly to rigid transformations and non-rigid bending of the raw 3D scan. This could be addressed in future work by leveraging deep learning techniques that would use larger datasets to learn intuitive and efficient cross-sectional encodings [34]. These techniques could also characterize shape variations across different regions in addition to the torso. Finally, the developed model did not capture the growth or longitudinal shape changes observed during pregnancy. This could be addressed in future studies by training a model on 3D scans of pregnant women across different gestational periods. Our eventual goal is to develop a point-of-care tool that uses statistical shape models to analyze, in real-time, the shape variations in 3D scans of pregnant women and assess the risk of CPD-related obstructed labor at the earliest possible stages of gestation.

V. CONCLUSION

This paper presents a fast, constrained optimization to parameterize 3D scans and uses the deformation parameters to build

a statistical model that represents the shape variations of the torso of pregnant women beyond 36 weeks of gestation. The model successfully characterized the shape changes of the torso of the pregnant population, adapted well to unobserved 3D scans, and accurately predicted various maternal anthropometric measurements with reduced inter-user variability.

REFERENCES

[1] S. B. Heymsfield, B. Bourgeois, B. K. Ng, M. J. Sommer, X. Li, and J. A. Shepherd, "Digital anthropometry: a critical review," *European journal of clinical nutrition*, vol. 72, no. 5, pp. 680–687, 2018.

[2] E. Mocini, C. Cammarota, F. Frigerio, L. Muzzioli, C. Piciocchi, D. Lacalaprice, F. Buccolini, L. M. Donini, and A. Pinto, "Digital anthropometry: A systematic review on precision, reliability and accuracy of most popular existing technologies," *Nutrients*, vol. 15, no. 2, p. 302, 2023.

[3] M. A. Minetto, A. Pietrobelli, C. Busso, J. P. Bennett, A. Ferraris, J. A. Shepherd, and S. B. Heymsfield, "Digital anthropometry for body circumference measurements: European phenotypic variations throughout the decades," *Journal of Personalized Medicine*, vol. 12, no. 6, p. 906, 2022.

[4] K. Bartol, D. Bojanić, T. Petković, and T. Pribanić, "A review of body measurement using 3d scanning," *Ieee Access*, vol. 9, pp. 67281–67301, 2021.

[5] S. Sobhiyeh, S. Kennedy, A. Dunkel, M. E. Dechenaud, J. A. Weston, J. Shepherd, P. Wolenski, and S. B. Heymsfield, "Digital anthropometry for body circumference measurements: Toward the development of universal three-dimensional optical system analysis software," *Obesity Science & Practice*, vol. 7, no. 1, pp. 35–44, 2021.

[6] L. Tolentino, M. Yigeremu, S. Teklu, S. Attia, M. Weiler, N. Frank, J. B. Dixon, and R. L. Gleason Jr, "Three-dimensional camera anthropometry to assess risk of cephalopelvic disproportion-related obstructed labour in ethiopia," *Interface Focus*, vol. 9, no. 5, p. 20190036, 2019.

[7] J. Conkle, P. S. Suchdev, E. Alexander, R. Flores-Ayala, U. Ramakrishnan, and R. Martorell, "Accuracy and reliability of a low-cost, handheld 3d imaging system for child anthropometry," *PloS one*, vol. 13, no. 10, p. e0205320, 2018.

[8] L. Soileau, D. Bautista, C. Johnson, C. Gao, K. Zhang, X. Li, S. Heymsfield, D. Thomas, and J. Zheng, "Automated anthropometric phenotyping with novel kinect-based three-dimensional imaging method: comparison with a reference laser imaging system," *European journal of clinical nutrition*, vol. 70, no. 4, pp. 475–481, 2016.

[9] N. Torres-Tamayo, S. Martelli, S. Schlager, D. García-Martínez, J. A. Sanchis-Gimeno, F. Mata-Escolano, S. Nalla, N. Ogihara, M. Oishi, and M. Bastir, "Assessing thoraco-pelvic covariation in homo sapiens and pan troglodytes: A 3d geometric morphometric approach," *American journal of physical anthropology*, vol. 173, no. 3, pp. 514–534, 2020.

[10] J.-M. Lu and M.-J. J. Wang, "Automated anthropometric data collection using 3d whole body scanners," *Expert Systems with Applications*, vol. 35, no. 1-2, pp. 407–414, 2008.

[11] B. Allen, B. Curless, and Z. Popović, "The space of human body shapes: reconstruction and parameterization from range scans," *ACM transactions on graphics (TOG)*, vol. 22, no. 3, pp. 587–594, 2003.

[12] N. Hasler, C. Stoll, M. Sunkel, B. Rosenhahn, and H.-P. Seidel, "A statistical model of human pose and body shape," in *Computer graphics forum*, vol. 28, pp. 337–346, Wiley Online Library, 2009.

[13] A. Weiss, D. Hirshberg, and M. J. Black, "Home 3d body scans from noisy image and range data," in *2011 International Conference on Computer Vision*, pp. 1951–1958, IEEE, 2011.

[14] A. Tsoli, M. Loper, and M. J. Black, "Model-based anthropometry: Predicting measurements from 3d human scans in multiple poses," in *IEEE winter conference on applications of computer vision*, pp. 83–90, IEEE, 2014.

[15] S. Yan, J. Wirta, and J.-K. Kämäräinen, "Anthropometric clothing measurements from 3d body scans," *Machine Vision and Applications*, vol. 31, no. 1-2, p. 7, 2020.

[16] D. Anguelov, P. Srinivasan, D. Koller, S. Thrun, J. Rodgers, and J. Davis, "Scape: shape completion and animation of people," in *ACM SIGGRAPH 2005 Papers*, pp. 408–416, 2005.

[17] M. Loper, N. Mahmood, J. Romero, G. Pons-Moll, and M. J. Black, "Smpl: A skinned multi-person linear model," *ACM transactions on graphics (TOG)*, vol. 34, no. 6, pp. 1–16, 2015.

[18] Z.-Q. Cheng, Y. Chen, R. R. Martin, T. Wu, and Z. Song, "Parametric modeling of 3d human body shape—a survey," *Computers & Graphics*, vol. 71, pp. 88–100, 2018.

[19] W. H. Organization *et al.*, *WHO recommendations on antenatal care for a positive pregnancy experience*. World Health Organization, 2016.

[20] R. L. Gleason Jr, M. Yigeremu, T. Debebe, S. Teklu, D. Zewdeneh, M. Weiler, N. Frank, L. Tolentino, S. Attia, J. B. Dixon, *et al.*, "A safe, low-cost, easy-to-use 3d camera platform to assess risk of obstructed labor due to cephalopelvic disproportion," *PloS one*, vol. 13, no. 9, p. e0203865, 2018.

[21] E. Arendt, N. S. Singh, and O. M. Campbell, "Effect of maternal height on caesarean section and neonatal mortality rates in sub-saharan africa: an analysis of 34 national datasets," *PLoS One*, vol. 13, no. 2, p. e0192167, 2018.

[22] A. Kelly, J. Kevany, M. De Onis, and P. Shah, "A who collaborative study of maternal anthropometry and pregnancy outcomes," *International Journal of Gynecology & Obstetrics*, vol. 53, no. 3, pp. 219–233, 1996.

[23] M. Thame, C. Osmond, F. Bennett, R. Wilks, and T. Forrester, "Fetal growth is directly related to maternal anthropometry and placental volume," *European journal of clinical nutrition*, vol. 58, no. 6, pp. 894–900, 2004.

[24] K. M. Robinette, H. Daanen, and E. Paquet, "The caesar project: a 3-d surface anthropometry survey," in *Second international conference on 3-D digital imaging and modeling (cat. No. PR00062)*, pp. 380–386, IEEE, 1999.

[25] F. Bogo, J. Romero, M. Loper, and M. J. Black, "Faust: Dataset and evaluation for 3d mesh registration," in *Proceedings of the IEEE conference on computer vision and pattern recognition*, pp. 3794–3801, 2014.

[26] M. R. Routzong, G. Rostaminia, P. A. Moalli, and S. D. Abramowitch, "Pelvic floor shape variations during pregnancy and after vaginal delivery," *Computer Methods and Programs in Biomedicine*, vol. 194, p. 105516, 2020.

[27] J. Verwaerde, J. Laforet, C. Marque, and A. Rassineux, "Statistical shape analysis of gravid uteri throughout pregnancy by a ray description technique," *Medical & Biological Engineering & Computing*, vol. 59, pp. 2165–2183, 2021.

[28] T. Möller and B. Trumbore, "Fast, minimum storage ray/triangle intersection," in *ACM SIGGRAPH 2005 Courses*, pp. 7–es, 2005.

[29] M. A. Styner, K. T. Rajamani, L.-P. Nolte, G. Zsemlye, G. Székely, C. J. Taylor, and R. H. Davies, "Evaluation of 3d correspondence methods for model building," in *Information Processing in Medical Imaging: 18th International Conference, IPMI 2003, Ambleside, UK, July 20-25, 2003. Proceedings 18*, pp. 63–75, Springer, 2003.

[30] M. Weiherer, A. Eigenberger, B. Egger, V. Brébant, L. Prantl, and C. Palm, "Learning the shape of female breasts: an open-access 3d statistical shape model of the female breast built from 110 breast scans," *The Visual Computer*, vol. 39, no. 4, pp. 1597–1616, 2023.

[31] L. Sigal, M. Isard, H. Haussecker, and M. J. Black, "Loose-limbed people: Estimating 3d human pose and motion using non-parametric belief propagation," *International journal of computer vision*, vol. 98, pp. 15–48, 2012.

[32] S. Zuffi and M. J. Black, "The stitched puppet: A graphical model of 3d human shape and pose," in *Proceedings of the IEEE Conference on Computer Vision and Pattern Recognition*, pp. 3537–3546, 2015.

[33] Z. Xue, D. Shen, and C. Davatzikos, "Statistical representation of high-dimensional deformation fields with application to statistically constrained 3d warping," *Medical image analysis*, vol. 10, no. 5, pp. 740–751, 2006.

[34] N. A. Dinh, H. Wang, G. Shakhnarovich, and R. Hanocka, "Loopdraw: a loop-based autoregressive model for shape synthesis and editing," *arXiv preprint arXiv:2212.04981*, 2022.

PLACE PHOTO HERE

LIKHIT K. NAYAK received the B.S. degree in Biomedical Engineering from Georgia Institute of Technology, Atlanta in 2018 and is currently pursuing his Ph.D. in Bioengineering at Georgia Institute of Technology, Atlanta. His research interests include applications of computational techniques in the domain of healthcare, design and development of point-of-care tools for resource-constrained settings, and global health innovations.

PLACE PHOTO HERE

MAHLET Y. GEBREMARIAM , MD is an academic faculty at the Department of Obstetrics and Gynecology, College of Health Sciences, Addis Ababa University, Ethiopia engaged in teaching undergraduate students and residents in obstetrics and gynecology since 2005. In 2012, Dr. Gebremariam was appointed as the Dean of School of Medicine at Addis Ababa University, Ethiopia and the CEO of Tikur Anbessa Specialized Hospital, Ethiopia. Her research interests are focused on understanding risk factors for maternal complications, like cephalopelvic disproportion (CPD) and preeclampsia, and developing clinical interventions for them.

PLACE PHOTO HERE

ELIANNA PALJUG received the B.S. degree in Biomedical Engineering from Georgia Institute of Technology, Atlanta in 2019, the M.S. degree in Bioengineering from Georgia Institute of Technology, Atlanta in 2021 and is currently pursuing an M.P.H. in Global Health at Emory University, Atlanta.

PLACE PHOTO HERE

RUDOLPH L. GLEASON received the B.S. degree in Environmental Engineering from the University of Florida, Gainsville in 1996, the M.S. degree in Mechanical Engineering from the University of Florida, Gainsville in 2000 and a Ph.D. degree in Biomedical Engineering from Texas A&M University, College Station. He is currently an Associate Professor with a Joint Appointment in the School of Mechanical Engineering and the School of Biomedical Engineering at Georgia Institute of Technology, Atlanta. Dr. Gleason's current research interests include tissue biomechanics, growth and remodeling of vascular tissues, and grand challenges in global health.

TABLE I. Average time taken for deformation and average deformation error for six different values of N_T.

N_T	$\Delta\theta_r$ (degrees)	Δy (m)	Average deformation time (s)	Average deformation error (m)
9090	4	0.02	14.80	0.0152
18090	4	0.01	29.12	0.0116
18180	2	0.02	29.87	0.0119
36090	4	0.005	58.22	0.0094
36180	2	0.01	58.03	0.0086
72360	1	0.01	114.21	0.0072

TABLE II. Mean of reconstruction error and reconstruction error % (calculated as (error / height) * 100) between original scan S, belonging to testing set, and reconstructed scan for the first k principal vectors.

k	Mean reconstruction error (m)	Mean reconstruction error %
10	0.0243	1.45%
25	0.0208	1.23%
50	0.0192	1.14%
100	0.0179	1.07%

TABLE III. Compactness, generalization, and specificity of statistical shape models built using the first k principal vectors. The generalization error was calculated as the average reconstruction error and the generalization error % was calculated as (generalization error / height) * 100

k	Ratio of explained variance	Generalization error (m)	Generalization error %	Specificity (m)
10	0.791	0.0398	2.36%	0.0324
25	0.904	0.0375	2.22%	0.0406
50	0.953	0.0363	2.15%	0.0483
100	0.983	0.0355	2.10%	0.0520

TABLE IV. Average error percentage of the predicted measurements, calculated as (error / actual anthropometric measurement) * 100, for eight different anthropometric measurements using two different values of N_T.

Anthropometric measurement	Average error % (N_T=9090)	Average error % (N_T=18090)
Height (cm)	2.98%	3.02%
Weight (kg)	10.19%	10.13%
Shoulder width (cm)	4.24%	4.26%
Shoulder height (cm)	3.59%	3.65%
Waist circumference (cm)	4.21%	4.20%
Waist height (cm)	3.81%	3.82%
Hip circumference (cm)	4.70%	4.67%
Trochanteric height (cm)	4.29%	4.31%

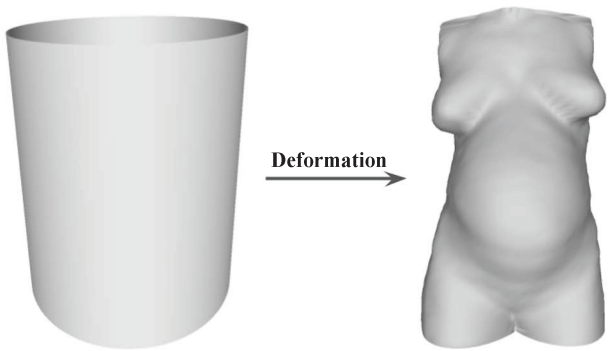

FIGURE 1. **Our method parameterizes a given scan by deforming a cylindrical template to fit the shape of the scan.**

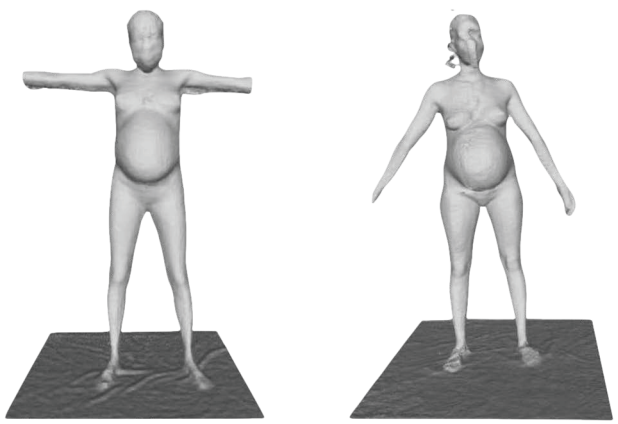

FIGURE 2. **The dataset consists of scans of women beyond 36 weeks of gestation collected in the standing posture with the position of the arms ranging from (a) T-Pose to (b) A-Pose.**

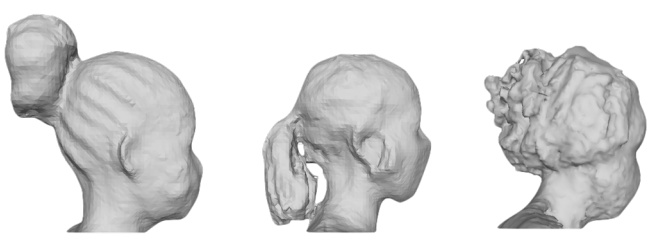

FIGURE 3. **The participants had their hair tied up in various styles and shapes. The head and neck regions were removed from all scans to prevent these variations from affecting our shape model.**

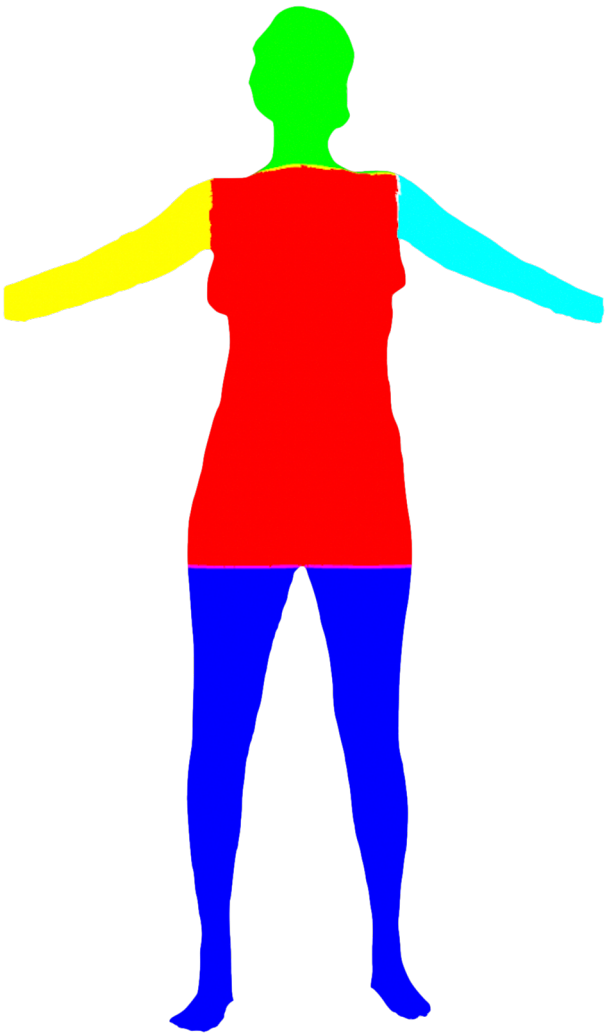

FIGURE 4. **Each scan was segmented into five regions - left arm (shown in cyan), right arm (shown in yellow), left and right legs (shown in blue), torso (shown in red) and head and neck (shown in green). Only the torso region was used for shape modelling.**

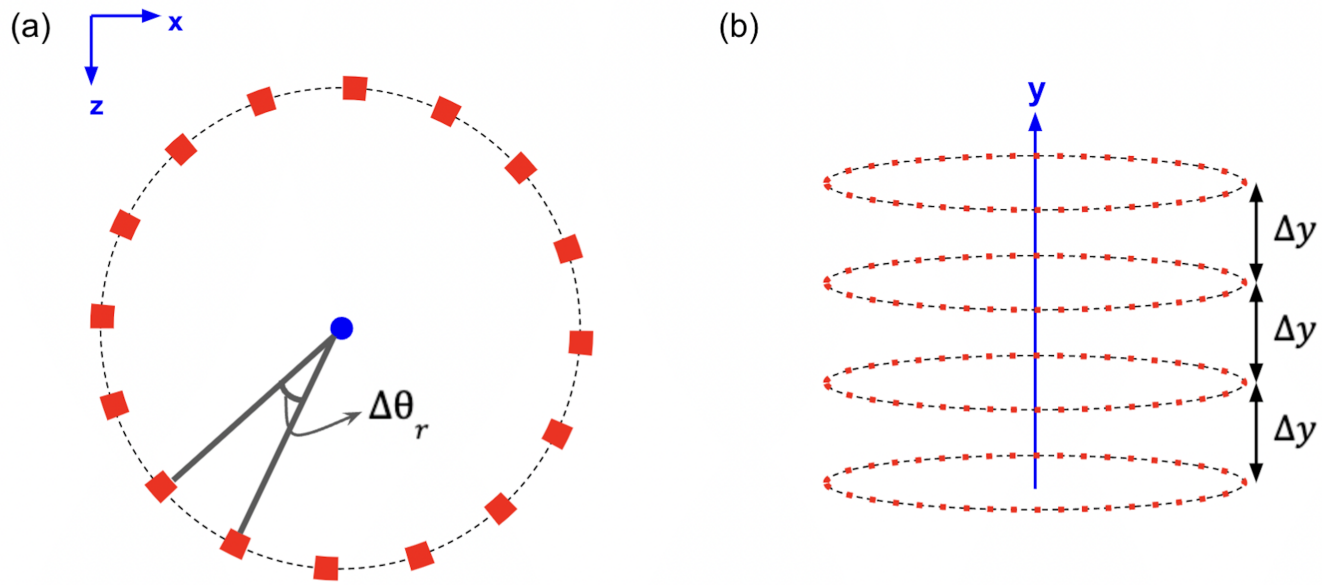

FIGURE 5. **(a) The angle θ_r subtended by neighboring vertices, depicted as red squares, on the same *xz* plane and (b) the cross-sectional distance *y* between individual *xz* planes**

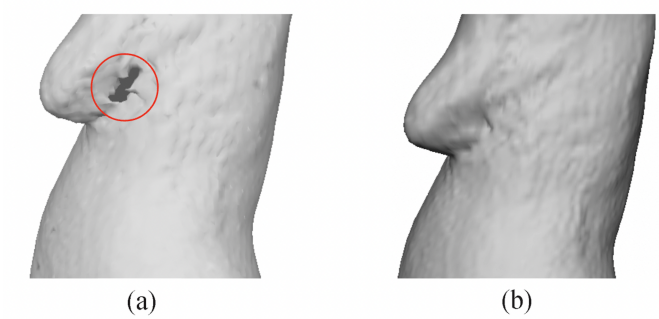

FIGURE 6. **The holes in the (a) raw scan are filled to give the (b) clean deformed template**

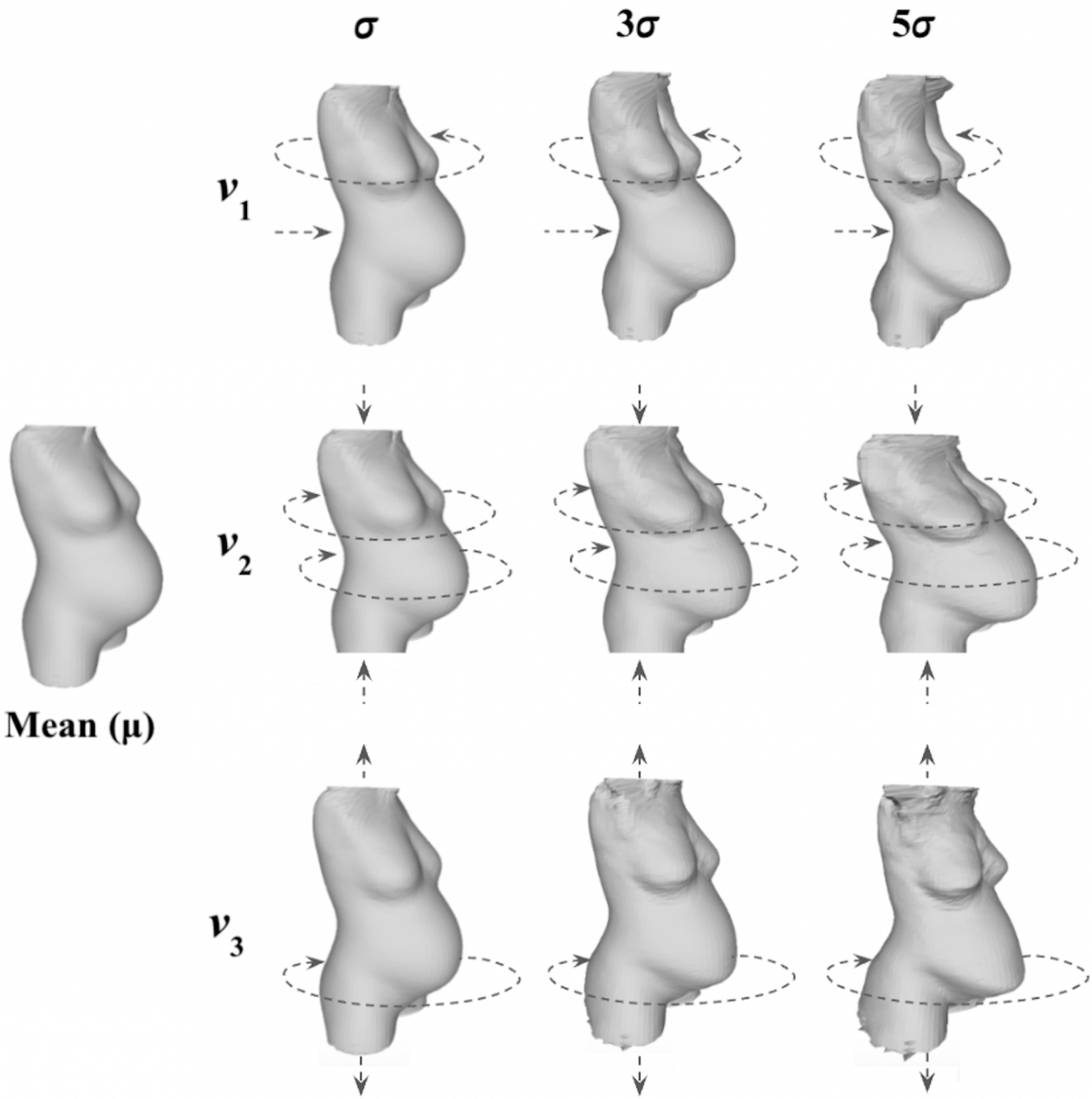

FIGURE 7. **Meshes showing deviations by one standard deviation (σ), three standard deviations (3σ) and five standard deviations (5σ) from the mean shape (μ) along each of the first three principal components (v_1, v_2, v_3).**

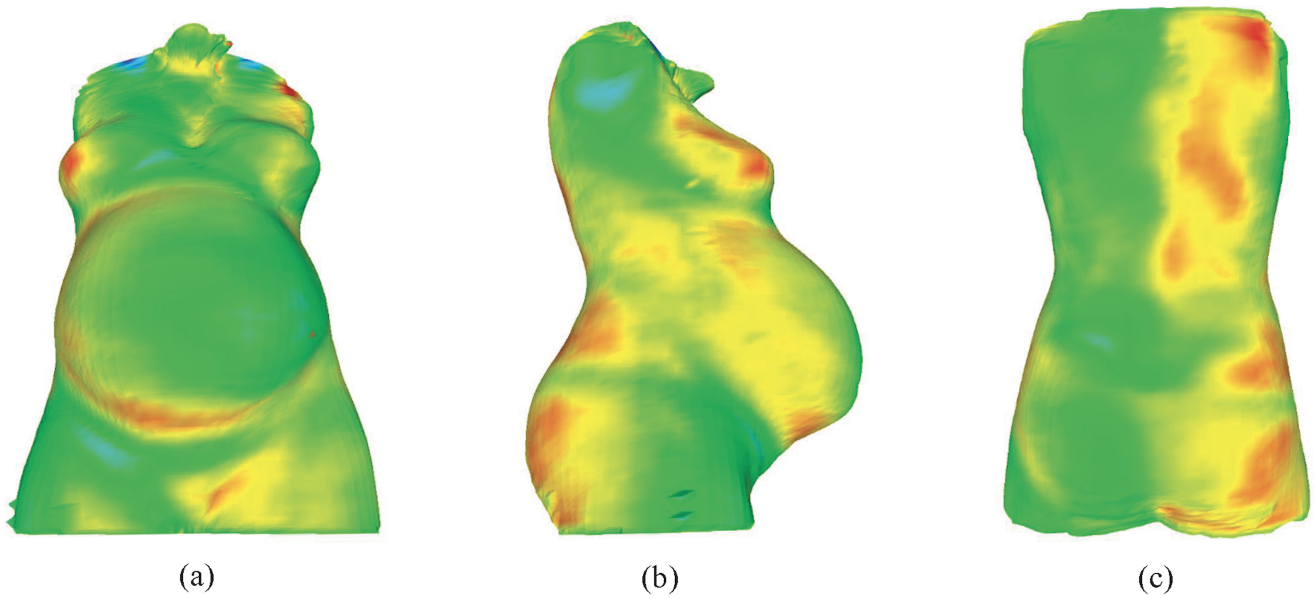

FIGURE 8. **Heat map of the Hausdorff distance from the original scanned mesh displayed on the mesh reconstructed using first 25 principal vectors from (a) front, (b) side, and (c) back views. The green areas had the lowest Hausdorff distance while the red areas had the highest Hausdorff distance.**

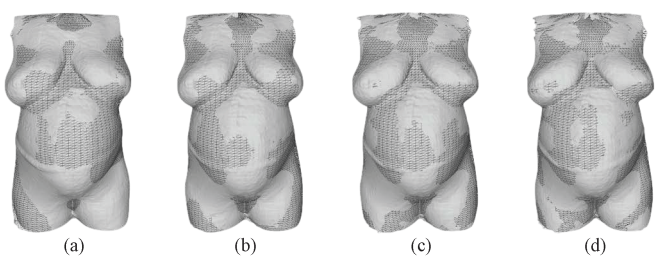

FIGURE 9. **The original scanned mesh (grey) overlaid on the reconstructed mesh (black wireframe) made using (a) first 10, (b) first 25, (c) first 50, and (d) first 100 principal vectors.**

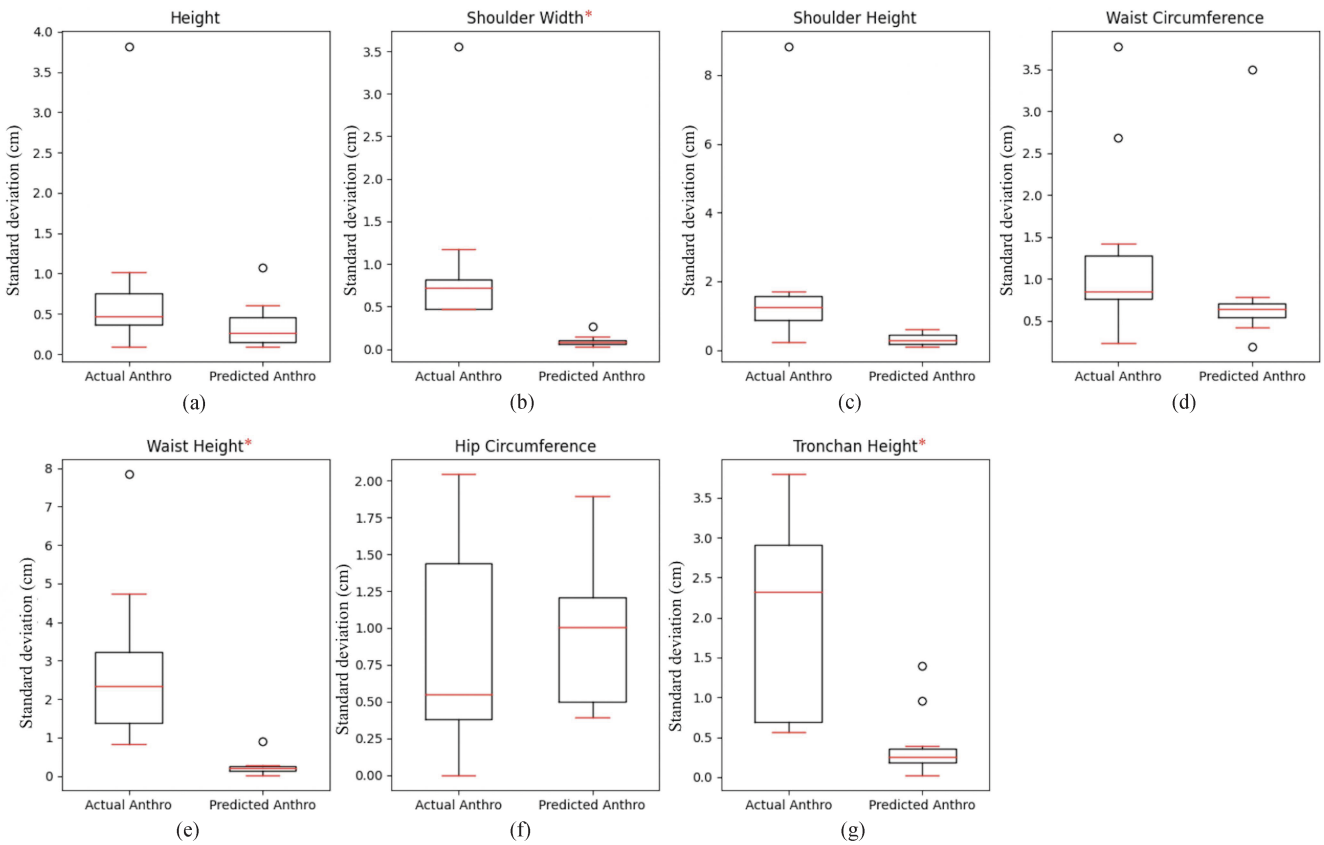

FIGURE 10. **Boxplots of the standard deviation of actual and predicted anthropometric measurements of (a) height, (b) shoulder width, (c) shoulder height, (d) waist circumference, (e) waist height, (f) hip circumference and (g) trochanteric height of each participant (n=12). The red asterisk (*) next to the plot title indicates a significant difference (p-value < 0.005) between the actual and predicted measurements.**